Experimental Thermal and Fluid Science 85 (2017) 257–265

Contents lists available at ScienceDirect

Experimental Thermal and Fluid Science

journal homepage: www.elsevier.com/locate/etfs

Surface coking deposition influences on flow and heat transfer of supercritical hydrocarbon fuel in helical tubes

Yanchen Fu, Jie Wen *, Zhi Tao, Guoqiang Xu, Haoran Huang

National Key Laboratory of Science and Technology on Aero-Engine Aero-thermodynamics, Collaborative Innovation Center of Advanced Aero-Engine, School of Energy and Power Engineering, Beihang University, Beijing 100191, China

ARTICLE INFO

Article history:
Received 12 November 2016
Received in revised form 19 February 2017
Accepted 11 March 2017
Available online 14 March 2017

Keywords:
Supercritical RP-3
Surface coking deposition
Helical tubes
Heat transfer
Pressure drop

ABSTRACT

Surface coking deposition influences on flow and heat transfer of aviation kerosene RP-3 in helical tubes were experimentally investigated at supercritical pressure. Four types of helical tubes with fixed pitch and various helical diameters have 1.86 mm inner diameter and 2.2 mm outer diameter. The system pressure, inlet temperature, mass flow rate were fixed at 5 MPa, 400 K and 1178 kg/m^2 s, respectively. The results indicate that the helical centrifugal force could inhibit the thermal oxidation coking and slow down the growth rate of press drop within maximum value of 47.6%. For the same cross section, the outer heat transfer coefficient (HTC) decreases gradually and eventually is less than the inner side due to coking deposition. Finally, a correlation of Nusselt number considering coking deposition was simulated to predict the heat transfer characteristics.

1. Introduction

With the increase of pressure ratio and turbine inlet temperature in modern aero engines, the cooling system for turbo components faces much more challenges. As the developments of new material and internal cooling technology could not satisfy the demand, one technology named CCA [1] (Cooled Cooling Air) is proposed to improve the cooling air quality and energy utilization rate. Hydrocarbon fuel would be used in the technology, heated and compressed in the supercritical status because the fuel feed system varies from 3.45 to 6.89 MPa in typical aero engines [2]. Thus, flow and heat transfer characteristics of hydrocarbon fuels at supercritical pressures are vital important in the CCA technology for advanced aero engines.

Previous researches on flow and heat transfer of supercritical fluid are mainly into pure liquid such as water and carbon dioxide. Jackson and Hall [3] investigated the heat transfer enhancement and deterioration mechanisms for supercritical fluid in different flow directions. Under the condition of heating, the buoyancy effect is reduced by the radial thermal property gradient due to the temperature difference between the inner wall and bulk. The buoyancy could influence the fluid shear force near the wall and then change the turbulence kinetic energy. This variation leads to the heat transfer enhancement or deterioration and flow resistance difference. Some criteria to evaluate the buoyancy in vertical tubes were proposed, such as $Gr_b/Re^{2.7} > 10$ [4] and $Bo^* = Gr^*/(Re^{3.425}Pr^{0.8})$ [5]. Many similar results were concluded that buoyancy could enhance the heat transfer in downward flow [6,7]. Furthermore, thermal acceleration was observed and heat transfer deterioration occurred due to the flow laminarization. Based on the air heat transfer in tubes, McEligot et al. [8] presented the dimensionless acceleration factor K_v to judge the thermal acceleration level. The results show that when $K_v \geqslant 4 \times 10^{-6}$, thermal acceleration could significantly influence the HTC and the level decreases to the same with laminar flow. What's more, Liao and Zhao [9,10] experimentally investigated convective heat transfer for supercritical carbon dioxide in miniature tubes and results show that heat transfer deterioration happens due to the buoyance effect in downward flow when the Reynolds number is higher than 10^5. In Jiang [11–14] recent researches, similar phenomena were observed and buoyancy significantly influences the heat transfer of supercritical carbon dioxide.

Compared with pure liquid, hydrocarbon fuel consists of thousands of components and some chemical reactions lead to complicated heat transfer characteristics during the heating process. Also, thermal oxidation coking would deposit on the inner surface to decrease the HTC between the flow and the wall. Krieger and Chen [15] adapted SF6 replacing aviation kerosene to research inlet Reynolds number, system pressure and flow direction influences on heat transfer characteristics at supercritical pressures. The results indicate that system pressure and flow direction almost have no

* Corresponding author.
E-mail address: wenjie@buaa.edu.cn (J. Wen).

http://dx.doi.org/10.1016/j.expthermflusci.2017.03.016
0894-1777/

Nomenclature

A	surface area
C_p	isobaric specific heat capacity ((kJ/kg) K)
d	diameter (m)
D	helical diameter (m)
G	mass flow rate (kg/(m^2·s))
H	enthalpy (kJ/kg)
h	heat transfer coefficient (kW/(m^2·K))
I	electrical current (A)
L	length (m)
m	mass flux (g/s)
Nu	Nusselt number
n	coil numbers
P	pressure (MPa)
Q	heat (W)
q	heat flux (kW/m^2)
$R(T)$	electronic resistivity (Ω·m)
r	radius (m)
T	temperature (K)
t	time (min)
Re	Reynolds number
U	voltage (V)

Greek

Φ	heat power (W)
ρ	density (kg/m^3)
μ	dynamic viscosity (Pa·s)
v	kinetic viscosity (m^2/s)
λ	thermal conductivity (W/(m·K))
ε	uncertainty

Subscripts

b	bulk
c	coking
i	inner
in	inlet
o	outer
out	outlet
pc	pseudo-critical
w	wall
x	local position

effects on heat transfer when Reynolds number is lower than 10^5. Four various heat transfer period were concluded in Li and Zhu [16] research for supercritical hydrocarbon fuel: normal heat transfer, heat transfer enhancement, heat transfer deterioration, second heat transfer enhancement. At present, almost all correlations related to supercritical fluid heat transfer are simulated based on water or carbon dioxide experimental data and bulk temperature, wall temperature or film temperature are defined as qualitative temperature. Dickinson and Welch [17] adopted Dittus-Boelter equation to compare with experimental data and found that there exists large errors when the bulk temperature comes to pseudo critical temperature. Krasnoshchekov and Protopopov [18] considered that the equation with property changes correction factor ρ_w/ρ_b and $\bar{C}_p/C_{pb}$ could simulate experimental data better. Above all, many kinds of correlations [19–22] are simulated and these does not show large difference due to the experimental factors, thermal load and buoyancy effects.

As fundamental research in CCA technology applied in aero engines, flow and heat transfer of aviation kerosene RP-3 in straight tubes at supercritical pressures have been deeply studied in our previous research [23–27]. Helical tube as one typical curved tube would be widely used in the future heat exchange component in CCA technology. Berger et al. [28], Shah and Joshi [29], Naphon and Wongwises [30] all summarized flow and heat transfer characteristics of common fluid flowing in curved tubes. Otherwise, mechanism of heat transfer for supercritical hydrocarbon fuel in helical tube is still unclear, especially when the inner wall surface starts to emerge thermal coking. To consider the real application for air-fuel heat exchanger in aero engines, flow and heat transfer with thermal oxidation coking influence of aviation kerosene RP-3 at supercritical pressure in helical tubes were experimentally researched in this paper.

2. Test facility

2.1. Experimental system

Supercritical fluid flow and heat transfer system in Beihang University is shown in Fig. 1. The whole system consists of four main sub-systems: fuel feeding system, heating system, sampling system and cooling separation system. The aviation kerosene was exported from the fuel tank and then would be removed impurities through filter. The main flowing path could be pumped to maximum 15 MPa by the infusion pump (SP6015,15 MPa, 0.01–600 mL/min). When the fuel pressure is larger than 10 MPa, the pump pressure could relief automatically to guarantee the system security and stability. Then the system absolute pressure was measured by a capacitance-type pressure transmitter (Model: Rosemount 3051CA4, ±0.15%) and controlled by the back pressure valve equipped at the path outlet. Furthermore, the pressure drop of test section was measured by capacitance-type pressure transmitter (Model: Rosemount 3051CD4, ±0.065%) set between the inlet and outlet of experimental tube. The mass flow rate was measured by a Coriolis-force flow-meter (Model: DMF-1-1, 0.15%, Sincerity) before the fuel flew into the pre-heating section. To achieve the required inlet temperature, two current powers (TN-KGZ01, 100 V, 200 A) were set on the stainless steel tube. The fuel was cooled down to 310 K by the water-fuel heat exchanger after flowing through the test section and then accumulated to the waste fuel barrels.

Experimental set-up has absolute pressure, differential pressure, temperature, mass flow rate, heating voltage and current measuring instruments and equipment. All the measured experimental data are output in the form of electrical signals. Signals are gathered by ADAM-4018 data acquisition, transformed by ADAM-4520 to several documents and stored in computer.

2.2. Test section

The experimental test section is stainless steel (1Cr18Ni9Ti) tube and all helical tubes have total length of 1800 mm. The test tube has 1.82 mm inner diameter and 2.2 mm outer diameter. Two 150 mm-length thermal insulation sections were set both in the inlet and outlet, and the middle 1500 mm length was bent to helical type as experimentally heated section. Four kinds of helical tubes with same pitch were manufactured in order to evaluate helical diameter effects on heat transfer and coking characteristics. Table 1 shows the detailed parameters of experimental helical tubes. The experimental section was connected to the system by silver weld special joint to reduce the local flow resistance. 30

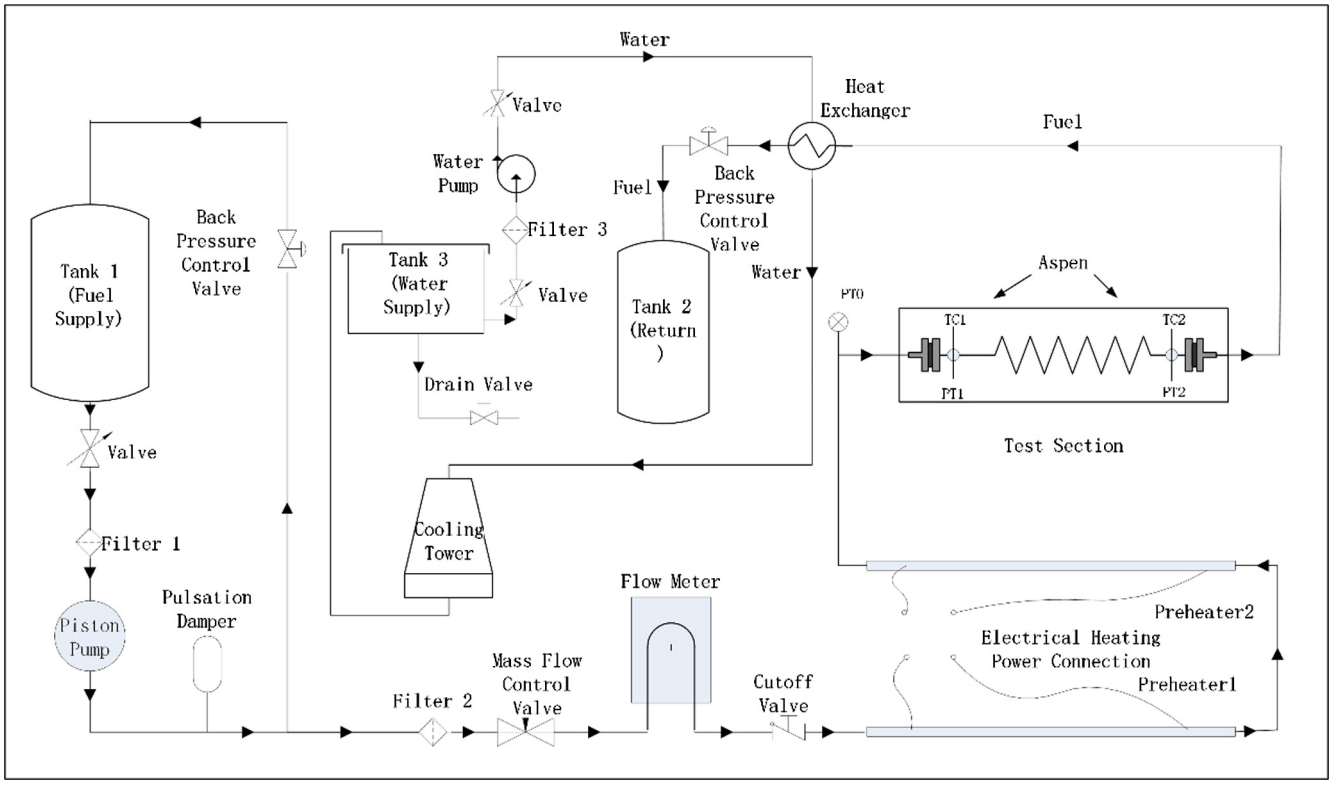

Fig. 1. Schematic of experimental system.

Table 1
Experimental helical tubes parameters.

Tube type	A	B	C	D
Helical diameter (mm)	502	118	67	46
Length of single coil (mm)	1500	372.9	214.3	149.9
Helix angle	1.5	6.2	10.8	15.5
Coil numbers	1	4	7	10
Pitch (mm)	40			
Length of helical section (mm)	1500			
Total length (mm)	1800			

NiCr-NiSi thermocouples were uniformly welded on the surface of helical tubes to monitor tube surface temperature variations. Basically, two thermocouples were set on the inner and outer position at the same dimensionless position to test the centrifugal force influences. In addition, all the test section was covered by Aspen thermal insulation material to reduce heat loss.

30 min oxygenation was applied in the fuel tank before each experiment to guarantee that the dissolved oxygen is in a saturated state and there is enough oxygen for coking reaction in the process of experiment. In order to keep the comparative experimental results at various working conditions, all system pressure conditions were set as 5 MPa and mass flow rate was from 393 kg/m^2 s to 1178 kg/m^2 s. The inlet fuel temperature was kept constant as 400 K, and outlet temperatures weas723 K at highest. To make contrast of time effects, experimental time was set to 1 h and 5 h.

2.3. Data and uncertainty analysis

Flow resistance of the experimental tube is evaluated by pressure drop between the inlet and outlet, and the value could be obtained directly by measurement. The local heat transfer for various position could be judged by local HTC h_x defined as following equation.

$$h_x = \frac{q_x}{T_{wx,i} - T_{b,x}} \tag{1}$$

q_x is the effective heat flux equal to the difference between electrical energy and heat losses. The following equation shows the electrical energy calculated by the current and tube electrical resistance.

$$q_x = \frac{I^2 R(T)[\pi(d_o^2 - d_i^2)/4]}{\pi d_i} - q_{x,loss} \tag{2}$$

where R(T) is the electronic resistivity of stainless steel tube. The heat loss is measured by power of preheating helical tube and simulated using temperature difference between tube surface and environment. As experimental tube have various types, each tube would have heat loss correction before experiments. The relationship among enthalpy of RP-3, fuel temperatures and the heating power could determine the local fuel temperature as follows.

$$T_b(x) = H^{-1}\left[\frac{Q_x}{\dot{m}} + H(T_{in})\right] \tag{3}$$

The inner wall temperature $T_{wx,i}$ was determined by solving the one-dimension thermal conductivity equation under the cylindrical coordinates system. The following equation could be obtained.

$$T_{wx,in} = T_{wx,out} - \left[\left(\Phi\frac{r_{out}^2}{2} - q_{x,loss} r_{out}\right)\ln\frac{r_{out}}{r_{in}} - \frac{\Phi}{4}(r_{out}^2 - r_{in}^2)\right] \Big/ \lambda_t \tag{4}$$

λ_t is the local thermal conductivity of stainless steel tube and $T_{wx,out}$ represents local outer wall temperatures in the test section. Finally, the local Nusselt number in helical tube is calculated by Eq. (5).

$$Nu_x = \frac{h_x d}{\lambda_f} \tag{5}$$

where λ_f is thermal conductivity of hydrocarbon fuel.

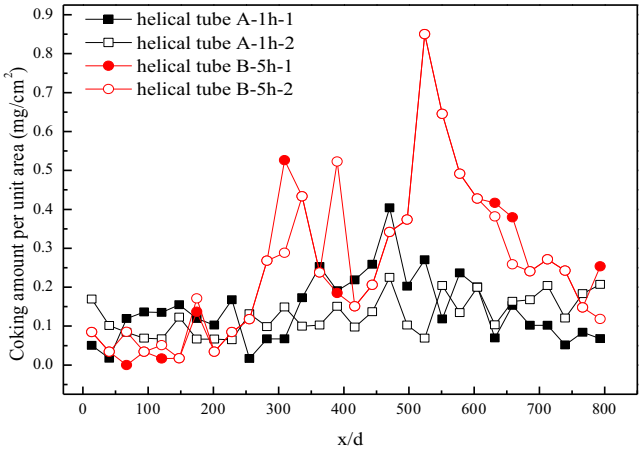

Fig. 2. Coking amount distribution for repeated experiments in helical tube A and B.

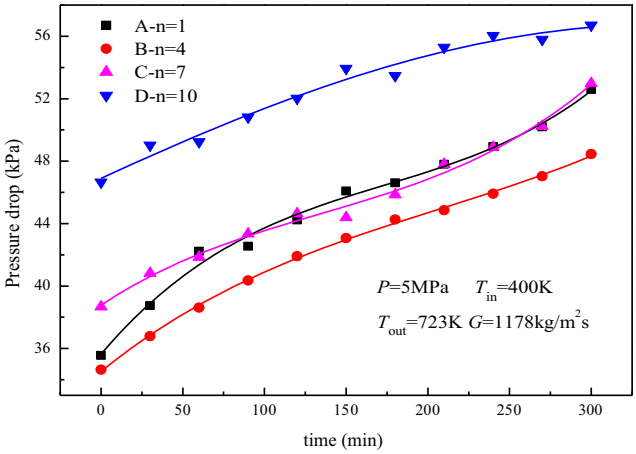

Fig. 3. Pressure drop variation along with time for four helical tubes.

According to experiments data in helical tubes, all the temperature differences between inner wall and fuel bulk are larger than 30 K. The uncertainties of local fuel bulk and inner wall temperatures are ±0.85 K and ±1.05 K, respectively. The following equation calculates the uncertainty of local heat flux and the value is 2.7%.

$$\left|\frac{\Delta q_x}{q_x}\right| = \sqrt{\left(\frac{q_x + q_{loss}}{q_x}\right)^2 \varepsilon^2(q_{0,x}) + \left(\frac{q_{loss,x}}{q_x}\right)^2 \varepsilon^2(q_{loss,x})} \quad (6)$$

Thus, the maximum uncertainties of local HTC and Nusselt number are confirmed as 5.2% and 6.0%, respectively.

2.4. Coke measurement and repeatability

Coking deposition distribution is one key factor to influence flow resistance and heat transfer characteristics. Weighing method is one common way to measure the coking deposition in previous research [31]. The measuring instrument was electronic analytical balance with the precision of 0.1 mg and each experimental helical tube would be cut uniformly into 30 pieces. There are twice weighs for each segment, firstly happened at the end of the experiment and secondly after the ultrasonic cleaning. Thus, the local coking deposition amount onto the inner surface was the difference value between two weighs.

Supercritical hydrocarbon fuel coking experiments need high accuracy for both coking amount measurement and heat transfer evaluation. Four experiments were conducted in helical tube A and B for 1 h and 5 h and all mass flow rate, inlet temperature, outlet temperature, and system pressure are identical. Fig. 2 shows the coking amount per unit area distributions in two helical tubes and it can be seen that the curve for two identical experiments are almost in coincidence. Also, the derivation of total coking amount for 1 h and 5 h experiments are 9.8% and 0.5%, respectively. Thus, coking amount repeatability of helical tube experiments could be checked.

3. Results and discussion

3.1. Flow resistance characteristics

As thermal oxidation coking produces and adheres onto the inner wall of tube during the heating process of supercritical aviation kerosene RP-3, inner wall roughness and tube diameter would be changed, and then flow resistance of the experimental tube would vary with the duration time. Fig. 3 displays pressure drop variations along with experimental time in four helical tubes. The working conditions are identical that system pressure is 5 MPa, mass flow rate is 1178 kg/m^2 s, inlet and outlet temperatures are 400 K and 723 K, respectively. It is seen from the figure that the pressure drop of helical tube D during the whole experimental is larger than those of other helical tubes. The main reason is that helical tube D has smaller helical diameter and more coil numbers. The larger centrifugal force induced by bending leads to larger local flow resistances under same working conditions.

For 5 h coking experiments, pressure drop of helical tubes all monotonically increases along with time in helical tubes A, B and C. In the early stage of experiment, the thermal oxidation coking starts to stick onto the inner tube surface and the roughness slowly increases. The mixing movement of hydrocarbon fuel in the wall layers strengths, which results in the increase of flow resistance differential pressure. However, the differential pressure growth rate keeps even as the same trend in the second half of experimental time, especially after 50 min. It is explained that various centrifugal force induced by different bending diameter is starting to lead the key role to influence the flow resistance. The effect of inner surface roughness gradually decreases and thermal coking began to change the fuel circulation area. Thus, the differential pressure drop increases slowly along with the time in various helical tubes. In addition, Fig. 4 shows the total coking amount for various helical tubes under identical working conditions. It is obvious that the maximum coking amount happens in helical A, which has the minimum coil numbers and maximum helical diameter. The differential pressure increases about 47.6% and far larger than

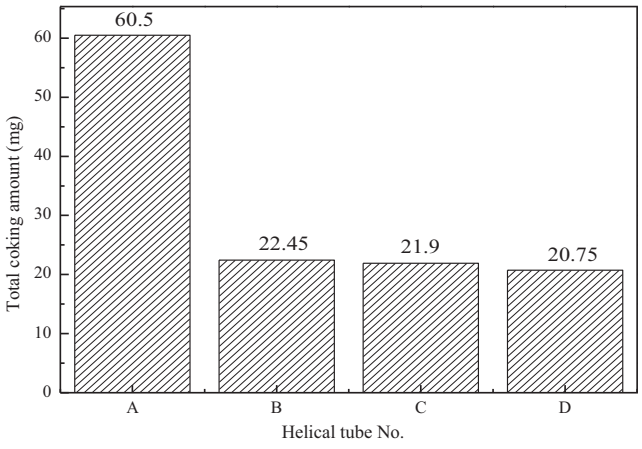

Fig. 4. Total coking amount for four helical tubes.

others. It is concluded that the coil number increase could inhibit the thermal oxidation coking and then slow down the growth of total differential pressure.

3.2. Convective heat transfer characteristics

Thermal oxidation coking along the tube distribution and coking morphologies for dimensionless positions vary with different helical tubes. Considering the influences of overall surface coking, fuel flow and heat transfer are mainly manifested on wall temperature and HTC variations. As the coking amount for 1 h experiment condition is small and coking layer thickness could hardly change the heat resistance, the following discussions are mainly about 5 h experiments.

3.2.1. Wall temperature distribution

Fig. 5 shows coking amount per unit area, fuel bulk and inner wall temperature variations in helical tube A. It can be seen that there exists one peak of inner wall temperature at the dimensionless position x/d = 480, corresponding to the coking amount peak. The coking rate per unit area has increased by about 10 times compared with the 1 h experiment. The centrifugal force induced by helical bending leads to the coking distribution more uniform and there exists less coking deposition at the inlet section due to the low fuel bulk temperature. At the outlet section, little part of coking precursor could accumulate there with the fuel flowing downward. Thus, the total wall coking amount slowly increases at the latter section of helical tube.

Furthermore, the coking peak makes the inner wall temperature varies from 668 K at the beginning to 757 K at the end of experiment. The inner wall coking increases the thermal resistance between wall and fuel bulk, leads to the heat transfer deterioration and increases the inner wall temperature. However, there is no significant variation for wall temperature in other sections during the whole experiment. Similar temperature and coking amount distribution happens at experiments in helical tubes B and C as shown in Figs. 6 and 7. The peaks of coking amount per unit area for two experimental tubes emerge at the dimensionless position between x/d = 510.8 and x/d = 537.6. The peak position has the trend of moving to the tube downstream with the increase of helical coil number. The main reason is that the dissolved oxygen could be held farther along with the fuel flowing and much more coking reactions happens at the latter area of the experimental tube.

In order to evaluate the centrifugal force effect on coking distribution on circumferential direction at the same position, two thermocouples were welded on the inner and outer spots for one tube cross section and 15 couples were distributed uniformly along the tube. The inner and outer temperature distributions for various dimensionless position of helical tube D are displayed in Fig. 8. It is demonstrated that both the inner and outer wall temperatures slowly changes along with time due to the relatively low average coking deposition at the dimensionless position x/d < 200. Also, the outer wall temperature varies from 669 K to 720 K in 5 h experiment, which is twice larger than the increase of inner wall temperature from 695 K to 707 K. This phenomenon indicates that thermal oxidation coking mainly concentrated on the outer side of circular cross section at the position of coking peak owing to the centrifugal force.

3.2.2. Heat transfer coefficient variation

Fig. 9 shows HTC variations along with experimental time in helical tube B. It is noted that the fuel bulk temperature is relatively low and small quantity of coking precursor deposits onto the inner surface at the dimensionless position of x/d = 0–245. Thus, the HTC at this section keeps gradually steady along with experimental time. At the section of coking peak, HTC decreases significantly as the coking deposition increases the thermal resistance. HTC worsening trend along with time gradually increases and obvious valley happens at the peak of coking rate. At the high temperature position section of x/d > 600, HTC firstly increases and then decreases along with experimental time. It can be explained that the cracking crystal block coking is divided into particles under the action of centrifugal force and then the mixing movement is strengthened between the internal wall and mainstream. However, the upstream dissolved oxygen is transported to promote the thermal oxidation coking during the experimental process, dense layer of coking is formed and HTC gradually decreases.

Helical diameter could influences the HTC distribution along with experimental time. Figs. 10–12 shows HTC variations along with time at different dimensionless positions for four helical tubes. At the low temperature section of x/d = 309.2, HTC tends to firstly increase and then gradually reduces. During the time period of t < 40 min, the HTC increase in helical tube D is relatively larger than others as the larger centrifugal force leads to the stronger turbulence effect at the entrance section. Fuel and dissolved oxygen reaction makes the coking adhere onto the inner wall and this

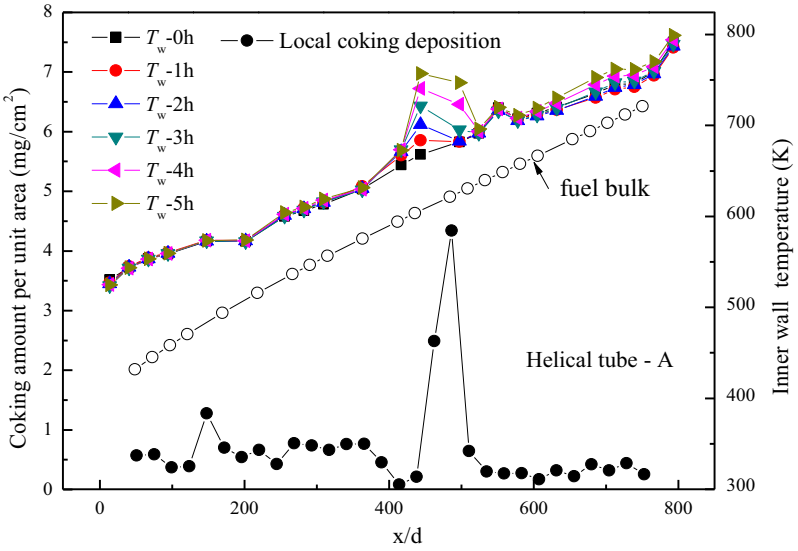

Fig. 5. Coking rate and inner wall temperature distribution for helical tube A.

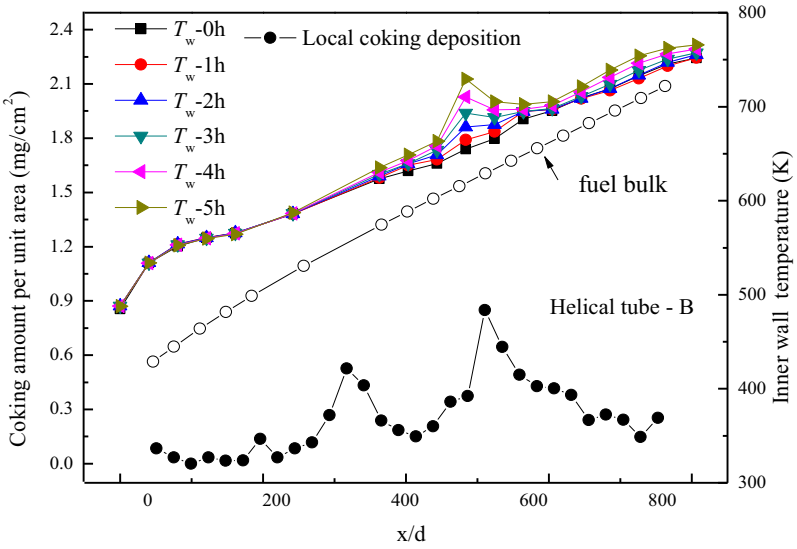

Fig. 6. Coking rate and inner wall temperature distribution for helical tube B.

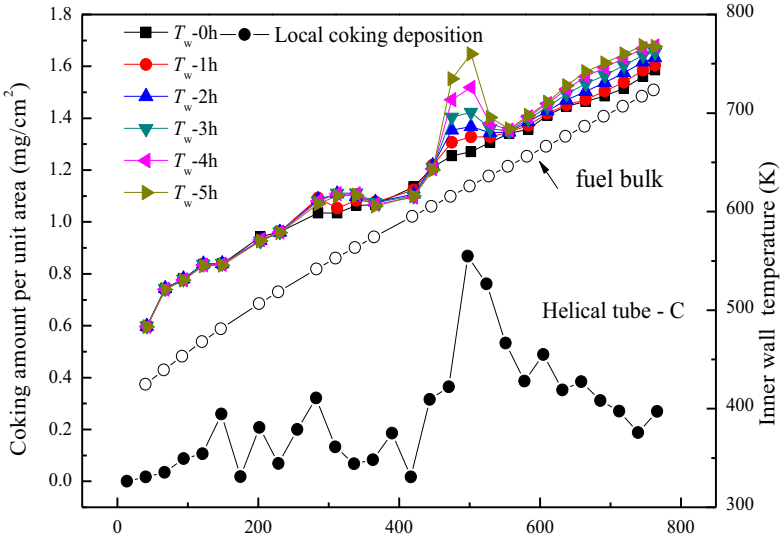

Fig. 7. Coking rate and inner wall temperature distribution for helical tube C.

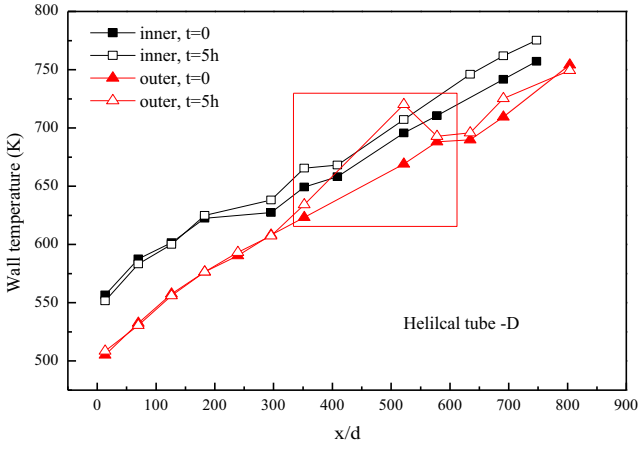

Fig. 8. Inner and outer wall temperature variation along with time at the same cross section.

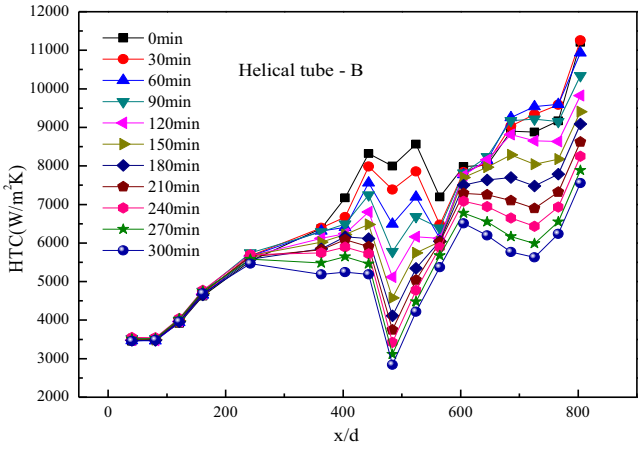

Fig. 9. Local heat transfer coefficient variation along with time for helical tube B.

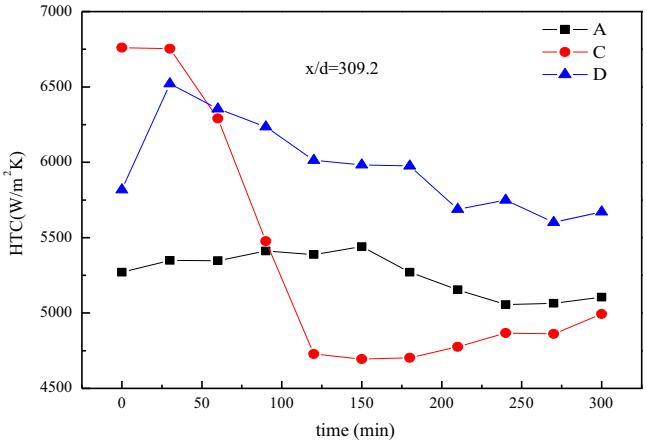

Fig. 10. Heat transfer coefficient variation at dimensionless position x/d = 309.2.

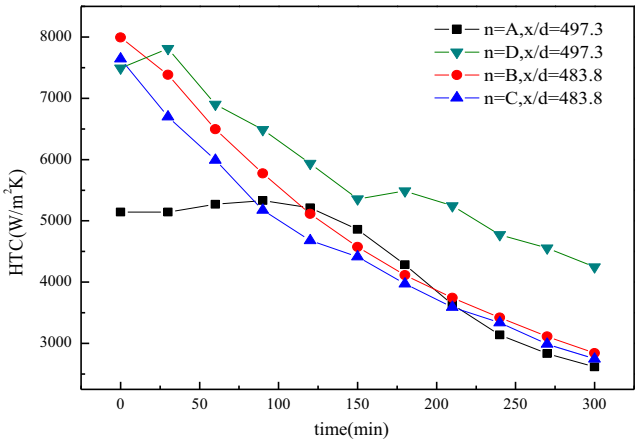

Fig. 11. Heat transfer coefficient variations at dimensionless positions x/d = 483.8 and 497.3.

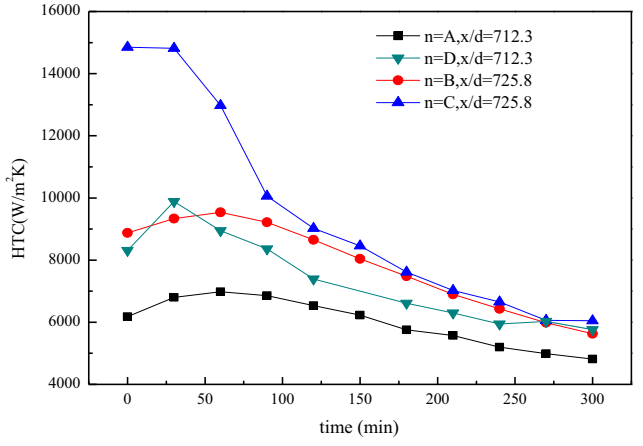

Fig. 12. Heat transfer coefficient variations at dimensionless positions x/d = 712.3 and 725.8.

enhances the wall surface roughness. With the experiment ongoing, the coking particles could fill in the porous media and thus increases the thermal resistances.

Coking rate peak happens at various dimensionless position for different tubes: x/d = 497.3 for helical tube A and D, x/d = 483.8 for helical tube B and C. It is displayed in Fig. 11 that the HTC of helical tube D is higher than others during the whole experiment. The reason is that centrifugal force starts to take the dominant role in heat transfer and thermal oxidation coking could not obviously influence the heat transfer. For helical tube A, coking precursor slowly deposits onto the inner wall and local HTC keeps steady in the period before 130 min. The helical diameter of tube B is similar to the diameter of tube C and centrifugal forces influencing the hydrocarbon fuel are in the same level. This results in the identical HTC variation that slowly decreases along with experimental time.

Fig. 12 shows the HTC variation at the high temperature section along with time for different helical tubes. In general, heat transfer affected by centrifugal force turbulence has been eliminated after 5 h high temperature coking process. As most of inner temperatures are higher than 723 K and the thermal cracking coking starts to emerge. The coking deposition could combine with the element Fe and Ni to form metallic carbide and that leads to the HTC slow decrease with time. Also, the helical tube C has the strongest ability to form thermal oxidation coking, which could be avoid applying in the further fuel-air heat exchanger design. Furthermore, inner and outer wall HTC variation differences at the same position is shown in Fig. 13. It is obvious that the outer HTC decreases by about 54.7% in 5 h, which is larger than 15.6% for inner side. The centrifugal force has the effect that much more coking deposits on the outer side than the inner side, especially after 230 min. Thus, coking distribution and heat transfer deterioration should be considered during the process of heat exchanger design.

3.2.3. Heat transfer correlation

Coking adhesion onto the inner wall surface could form the coking layer thermal resistance. The experimental thermal resistance between the tube wall and the mainstream fuel is obtained as follows based on the concept of thermal conductivity.

$$R = \frac{1}{K} = \frac{1}{2\pi\lambda_c} \ln\left(\frac{r_o}{r_i}\right) + \frac{1}{h_0}\frac{A_o}{A_i} \tag{7}$$

The above equation is established in terms of three assumptions: (1) Tube coking onto the inner wall is uniformly distributed along the helical tube axial directions. (2) Coking thickness variation could not affect the HTC, as the accurate coking thickness (r_o-r_i) and coking thermal conductivity are not measured. (3) When HTC reaches the highest peak, coking layer surface roughness, thermal physical properties such as thermal conductivity and density could not change with time any more.

In order to better evaluate the heat transfer deterioration caused by thermal oxidation coking, the following formula is pre-

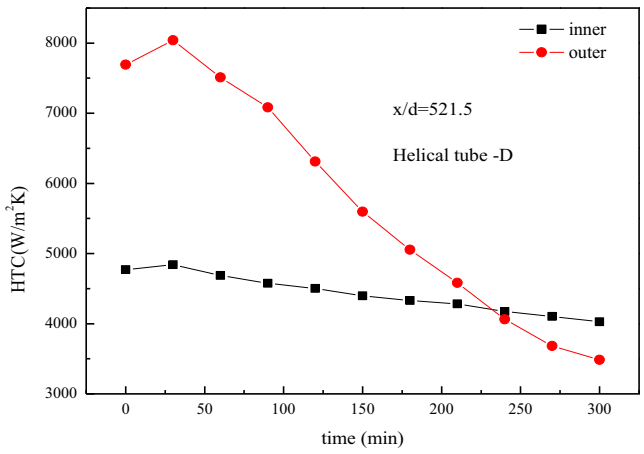

Fig. 13. Inner and outer heat transfer coefficient variation along with time at x/d = 521.5.

sented considering relationship among Nusselt numbers, axial position, experimental time, helical curvature and temperatures.

$$\frac{Nu}{Nu_0} = a\left(e^{\frac{t}{t_0}}\right)^b \left(e^{\frac{T_{wx,in}}{T_{bx}}}\right)^c \left(e^{\frac{x}{L}}\right)^d \left(e^{\frac{d_{in}}{D}}\right)^f \quad (8)$$

where Nu_0 is the Nusselt number at the starting point, t_0 is experimental time 300 min. D represents helical diameter, L is helical tube length, $T_{wx,in}$ and T_{bx} represent inner wall and fuel bulk temperatures, respectively. All experimental data at the mass flow rate condition of 1178 kg/m^2 s are analyzed and simulated using nonlinear fitting method, and the formula could be transferred as follows.

$$\frac{Nu}{Nu_0} = \exp\left(2.594 - 0.147\frac{t}{t_0} - 2.059\frac{T_{wx,in}}{T_b} - 0.530\frac{x}{L} - 1.425\frac{d_{in}}{D}\right) \quad (9)$$

Fig. 14 displays the comparison between experimental data and calculated results using above correlation. The results show that the experimental data and the values calculated by fitting correlation match well. The average relative error and maximum relative error are 8.71% and 24.6%, respectively. Also, all 881 experimental points are in the 25% error band and 93.9% of all points falls in the 20% error band. Hence, this correlation could be adopted in preliminary evaluation in the thermal oxidation coking of air-fuel heat exchanger design, and it has very important reference value for the application of CCA technology.

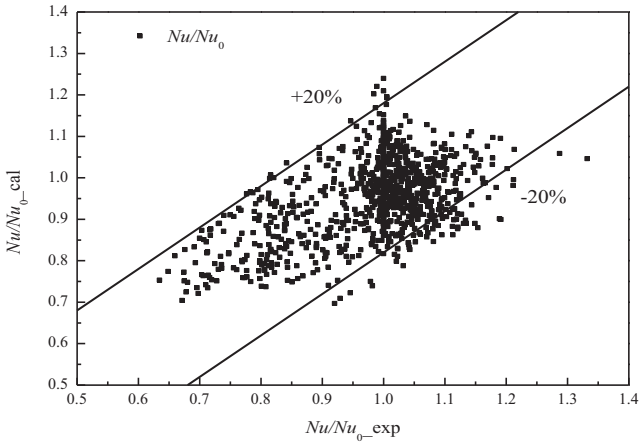

Fig. 14. Comparison between calculated Nusselt numbers and experimental data.

3.3. Thermal coking characteristics

Scanning Electron Microscope (SEM) was applied to detect the morphology of thermal oxidation coking. Fig. 15 shows inner wall coking characteristics of two positions after experiments in helical tubes B and C. Also, various coking elements quality percentages on the inner surface at the position of coking peak and high temperature outlet section are presented in Table 2. Thermal oxidation coking happening in helical tubes B and C have similar morphologies at dimensionless position between x/d = 510.8 and 537.6. C element content is about 80%, most of the rest is element O and no trace elements are found there. It demonstrates that the dissolved oxygen does not run out at the position of coking peak, and transported to the high temperature area along with mainstream to continue participating thermal coking reactions.

Section B-(2) and C-(2) are high temperature reaction areas for two helical tubes. Most parts of these two sections have inner wall temperature beyond 725 K, higher than the pseudo-critical and

Table 2
Various elements contents for inner surface coking section in helical tubes B and C.

Mass (%)	B-(1)	B-(2)	C-(1)	C-(2)
C	78.11	43.52	82.67	32.88
O	21.89	12.55	15.55	14.06
Fe		21.18		23.5
Cr		18.85		20.39
Mn		0.59		
Si		1.99	1.78	1.36
S		1.32		2.33
Zn				5.48

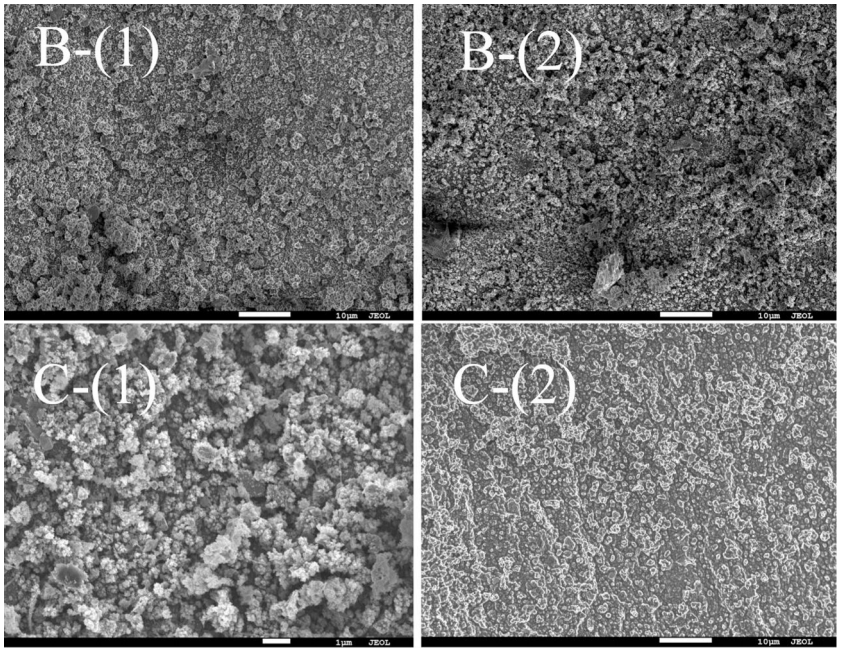

Fig. 15. Inner wall surface coking morphology in helical tubes B and C for various dimensionless positions. B: (1) x/d = 510.8–537.6, (2) x/d = 725.8–752.7; C: (1) x/d = 510.8–537.6, (2) x/d = 725.8–752.7.

thermal cracking temperatures. There exists thermal cracking reactions near the wall layer, the dense oxidation coking is destroyed and appears loose layer of flocculent precipitate. Moreover, the region existing elements of Fe and Cr contents in stainless steel obviously decreased compared with un-experimental tube. The reason is that the coking distribution is more dispersed due to the less quantity pyrolysis coking during high temperature period and short time working conditions.

4. Conclusion

Flow and heat transfer characteristics of supercritical hydrocarbon fuel considering surface coking deposition influences in four types of helical tubes have been experimentally investigated in this paper. Detailed wall temperature, HTC distribution and coking morphologies were obtained for various helical tubes and working conditions. Some key conclusions were made as follows:

(1) The decrease of helical diameter could strength centrifugal force, and then total coking amount is inhibited to slow down the growth of total pressure drop. The maximum pressure drop increase is about 47.6% in helical tube A.
(2) For all test tubes, HTC presents firstly increase and secondly decreases along with time. Different coking morphology reflects various heat transfer characteristics.
(3) Centrifugal force motives more coking deposit onto the outer side than the inner side. Thus, the outer HTC decreases gradually and eventually is less than the inner side.
(4) Correlation of Nusselt numbers for all 5 h experiments is simulated and 93.9% of calculated values are in the 20% error band.

Acknowledgement

The authors would like to acknowledge the financial support provided by the China National Natural Science Foundation (Grant No. 51606179).

References

[1] G. Bruening, W. Chang, Cooled Cooling Air Systems for Turbine Thermal Management, ASME Paper, (99-GT), 1999, p. 14.
[2] T. Edwards, S. Zabarnick, Supercritical fuel deposition mechanisms, Ind. Eng. Chem. Res. 32 (12) (1993) 3117–3122.
[3] W. Hall, Heat transfer near the critical point, Adv. Heat Transfer 7 (1971) 1–86.
[4] G. Adebiyi, W. Hall, Experimental investigation of heat transfer to supercritical pressure carbon dioxide in a horizontal pipe, Int. J. Heat Mass Transfer 19 (7) (1976) 715–720.
[5] J. Jackson, W. Hall, Forced convection heat transfer to fluids at supercritical pressure, Turbul Forced Convect Chan Bund 2 (1979) 563–611.
[6] F. J., Mixed Forced and Free Convective Heat Transfer to Supercritical Pressure Fluids Flowing in Vertical Pipes, The University of Manchester, 1976.
[7] J. Jackson, M. Cotton, B. Axcell, Studies of mixed convection in vertical tubes, Int. J. Hat Fluid Fl. 10 (1) (1989) 2–15.
[8] D. McEligot, C. Coon, H. Perkins, Relaminarization in tubes, Int. J. Heat Mass Transfer 13 (2) (1970) 431–433.
[9] S. Liao, T. Zhao, An experimental investigation of convection heat transfer to supercritical carbon dioxide in miniature tubes, Int. J. Heat Mass Transfer 45 (25) (2002) 5025–5034.
[10] S.M. Liao, T.S. Zhao, Measurements of heat transfer coefficients from supercritical carbon dioxide flowing in horizontal mini/micro channels, J. Heat Trans. – Trans. ASME 124 (3) (2002) 413.
[11] P. Jiang, Y. Zhang, R. Shi, Experimental and numerical investigation of convection heat transfer of CO_2 at super-critical pressures in a vertical mini tube, in: ASME 4th International Conference on Nanochannels, Microchannels, and Minichannels, American Society of Mechanical Engineers, 2006, pp. 583–590.
[12] P.-X. Jiang, R.-F. Shi, Y.-J. Xu, S. He, J. Jackson, Experimental investigation of flow resistance and convection heat transfer of CO_2 at supercritical pressures in a vertical porous tube, J. Supercrit. Fluid 38 (3) (2006) 339–346.
[13] P.-X. Jiang, Y. Zhang, Y.-J. Xu, R.-F. Shi, Experimental and numerical investigation of convection heat transfer of CO_2 at supercritical pressures in a vertical tube at low Reynolds numbers, Int. J. Therm. Sci. 47 (8) (2008) 998–1011.
[14] P.-X. Jiang, B. Liu, C.-R. Zhao, F. Luo, Convection heat transfer of supercritical pressure carbon dioxide in a vertical micro tube from transition to turbulent flow regime, Int. J. Heat Mass Transfer 56 (1) (2013) 741–749.
[15] J.R. Krieger, L.-D. Chen, Measurements of heat transfer to near-critical fluids, in: AIAA/ASME/SAE/ASEE Joint Propulsion Conference & Exhibit, 33 rd, Seattle, WA, 1997.
[16] Z. Li, H. Zhu, Heat transfer characteristics of kerosene in micro-channel under supercritical pressure, J. Propul. Tech. 32 (2) (2011) 261–265.
[17] N. Dickinson, C. Welch, Heat transfer to supercritical water, Trans. Am. Soc. Mech. Eng. 80 (1958).
[18] E. Krasnoshchekov, V. Protopopov, Experimental study of heat exchange in carbon dioxide in the supercritical range at high temperature drops (Heat transfer in turbulent carbon dioxide pipeflow at supercritical region), High Temp. 4 (1966) 375–382.
[19] P.A. Masters, C. Aukerman, Deposit Formation in Hydrocarbon Rocket Fuels with an Evaluation of a Propane Heat Transfer Correlation, AIAA Paper, 1290, 1982.
[20] J. TeVelde, M. Glickstein, Heat Transfer and Thermal Stability of Alternative Aircraft Fuels, US Naval Air Propulsion Center, Trenton, NJ, Report No. NAPC-PE-87C, 1983.
[21] R.N. Hazlett, Thermal Oxidation Stability of Aviation Turbine Fuels, ASTM, Philadelphia, 1991.
[22] B. Stiegemeier, M. Meyer, R. Taghavi, A thermal stability and heat transfer investigation of five hydrocarbon fuels, in: 38th AIAA/ASME/SAE/ASEE Joint Propulsion Conference & Exhibit, AIAA, 2002, pp. 1–10.
[23] H. Deng, K. Zhu, G. Xu, Z. Tao, J. Sun, Heat transfer characteristics of RP-3 kerosene at supercritical pressure in a vertical circular tube, J. Enhanc. Heat Transfer 19 (5) (2012).
[24] K. Zhu, G.-Q. Xu, Z. Tao, H.-W. Deng, Z.-H. Ran, C.-B. Zhang, Flow frictional resistance characteristics of kerosene RP-3 in horizontal circular tube at supercritical pressure, Exp. Therm. Fluid Sci. 44 (2013) 245–252.
[25] Z. Tao, Y. Fu, G. Xu, H. Deng, Z. Jia, Experimental study on influences of physical factors to supercritical RP-3 surface and liquid-space thermal oxidation coking, Energy Fuels 28 (9) (2014) 6098–6106.
[26] Z. Tao, Y. Fu, G. Xu, H. Deng, Z. Jia, Thermal and element analyses for supercritical RP-3 surface coke deposition under stable and vibration conditions, Energy Fuels 29 (3) (2015) 2006–2013.
[27] C. Zhang, G. Xu, L. Gao, Z. Tao, H. Deng, K. Zhu, Experimental investigation on heat transfer of a specific fuel (RP-3) flows through downward tubes at supercritical pressure, J. Supercrit. Fluid 72 (2012) 90–99.
[28] S. Berger, L. Talbot, L. Yao, Flow in curved pipes, Annu. Rev. Fluid Mech. 15 (1) (1983) 461–512.
[29] R. Shah, S. Joshi, Convective heat transfer in curved ducts, Handbook Single-Phase Convect. Heat Transfer 5 (3–5) (1987) 47.
[30] P. Naphon, S. Wongwises, A review of flow and heat transfer characteristics in curved tubes, Renew. Sust. Energy Rev. 10 (5) (2006) 463–490.
[31] K. Zhu, Z. Tao, G. Xu, Z. Jia, Surface deposition characteristics of supercritical kerosene RP-3 fuel within treated and untreated stainless-steel tubes. Part 1: Short thermal duration, Energy Fuels 30 (4) (2016) 2687–2693.